

# Magnetotransport in low-density $p$ -Si/SiGe heterostructures: From metal through hopping insulator to Wigner glass

I. L. Drichko,<sup>1,\*</sup> A. M. Dyakonov,<sup>1</sup> I. Yu. Smirnov,<sup>1</sup> A. V. Suslov,<sup>2</sup>  
Y. M. Galperin,<sup>3,1,4</sup> V. Vinokur,<sup>4</sup> M. Myronov,<sup>5</sup> O. A. Mironov,<sup>6</sup> and D. R. Leadley<sup>7</sup>  
<sup>1</sup>*A. F. Ioffe Physico-Technical Institute of Russian Academy of Sciences, 194021 St. Petersburg, Russia*  
<sup>2</sup>*National High Magnetic Field Laboratory, Tallahassee, FL 32310, USA*  
<sup>3</sup>*Department of Physics and Center for Advanced Materials and Nanotechnology,  
University of Oslo, PO Box 1048 Blindern, 0316 Oslo, Norway*  
<sup>4</sup>*Argonne National Laboratory, 9700 S. Cass Av., Argonne, IL 60439, USA*  
<sup>5</sup>*Musashi Institute of Technology, 8-15-1 Todoroki, Setagaya-ku, Tokyo, Japan*  
<sup>6</sup>*Warwick SEMINANO R&D Centre, University of Warwick Science Park, Coventry CV4 7EZ, UK*  
<sup>7</sup>*Department of Physics, University of Warwick, Coventry CV4 7AL, UK*

(Dated: October 25, 2018)

We study DC and AC transport in low-density  $p$ -Si/SiGe heterostructures at low temperatures and in a broad domain of magnetic fields up to 18 T. Complex AC conductance is determined from simultaneous measurement of velocity and attenuation of a surface acoustic wave propagating in close vicinity of the 2D hole layer. The observed behaviors of DC and AC conductance are interpreted as an evolution from metallic conductance at  $B = 0$  through hopping between localized states in intermediate magnetic fields (close to the plateau of the integer quantum Hall effect corresponding to the Landau-level filling factor  $\nu=1$ ) to formation of the Wigner glass in the extreme quantum limit ( $B \gtrsim 14$ ,  $T \lesssim 0.8$  K).

PACS numbers: 73.23.-b, 73.50.Rb, 73.43.-f, 73.43.Qt

## I. INTRODUCTION

Electron transport through two-dimensional (2D) semiconductor structures attracts great attention during many years. Firstly, two-dimensional layers serve as building blocks for devices of modern micro- and nano-electronics. Secondly, two-dimensional structures allow addressing several fundamental problems. In particular, they provide possibilities to analyze interplay between the electron-electron interaction and disorder, which is the most fundamental problem of modern condensed matter physics. External magnetic field adds a “new dimension” to these studies. A parallel magnetic field acts mostly upon spin degrees of freedom causing splitting of the electron levels corresponding to different spins. A perpendicular magnetic field acts mostly upon orbital degrees of freedom by shrinking electron wave functions. As a result, it influences the interaction-disorder interplay in a controlled way.

The most remarkable magneto-transport phenomena existing only in 2D systems are the integer and fractional quantum Hall effects (IQHE and FQHE, respectively). While the FQHE can be observed only in very pure samples having extremely high mobility, the IQHE is a typical feature of relatively disordered structures. Furthermore, according to conventional picture of the IQHE (see, e. g., Ref. 1 for a review), it is the disorder responsible for the “reservoir” of localized states which controls the evolution of the chemical potential with variation of the electron/hole density or magnetic field. The localized states, in turn, lead to broad plateaus in the dependence of the Hall component,  $\rho_{xy}$ , of the conductance tensor on magnetic field or electron density, and vanishing of the

transverse component,  $\rho_{xx}$ , at the plateaus. As usual, we assume that magnetic field is parallel to the  $\mathbf{z}$ -axis while the electric field is parallel to the  $\mathbf{x}$ -axis.

According to quantum mechanics,<sup>2</sup> the orbital energy spectrum of a perfect 2D electron system in a perpendicular magnetic field consists of discrete Landau levels (LLs),  $\varepsilon_n = \hbar\omega_c(n + 1/2)$  where  $\omega_c = eB/m^*c$  is the cyclotron frequency;  $B$  is the external magnetic field,  $e$  is the electron charge,  $m^*$  is the (cyclotron) effective mass, while  $c$  is the light velocity. The degeneracy factor of the levels is just the ratio between the sample area,  $A$ , and the effective area  $2\pi l_B^2$  occupied by a quantum state. Here  $l_B \equiv (\hbar c/eB)^{1/2}$  is the so-called Landau or magnetic length. The filling factor,  $\nu = 2\pi p l_B^2 = pch/eB$ , has a meaning of the ratio of the electron number to the “capacity” of a Landau level. Here  $p$  is the sheet electron/hole density. An integer  $\nu$  means that an integer number of LLs are fully occupied and the chemical potential is located in the gap between them. In the above consideration, we have defined the filling factor *per electron spin*. The external field causes Zeeman splitting,  $g^* \mu_B B$ , of the levels corresponding to different spins where  $\mu_B$  is the Bohr magneton while  $g^*$  is the so-called  $g$ -factor. If Zeeman splitting exceeds the thermal splitting,  $k_B T$ , then the spin-split levels are well resolved. Here  $T$  is temperature while  $k_B$  is the Boltzmann constant.

The domain where  $\nu < 1$  and  $k_B T \lesssim \hbar\omega_c$  is called the *extreme quantum limit* (EQL). In this domain the electron states are spin-polarized and only the lowest Landau level is partly occupied. The magneto-transport in the EQL region is far from being fully understood. There exist predictions that a 2D system in such situation be-

has as a specific ‘‘Hall insulator’’ where the off-diagonal component,  $\rho_{xy}$ , of the resistivity tensor keeps its classical values while the diagonal component,  $\rho_{xx}$ , diverges at zero temperature.<sup>3</sup>

This is in contrast with an ordinary (Anderson or Mott) insulator where both components diverge. Transverse DC conductance of both the Hall and an ordinary insulator at finite temperature is due to the variable-range hopping of electrons (holes) between localized states. It turns out that AC conductivity in this regime is complex,  $\sigma^{\text{AC}} \equiv \sigma_1 - i\sigma_2$  and  $\sigma_2 > \sigma_1 > \sigma_{xx}^{\text{DC}} = \rho_{xx}/(\rho_{xx}^2 + \rho_{xy}^2)$ .<sup>4</sup> This relation has been experimentally confirmed in GaAs/AlGaAs heterostructures near the conductivity minima in the IQHE regime using probeless acoustic methods to measure AC conductivity.<sup>5</sup> The observed large value of the ratio  $\sigma_2/\sigma_1$  was interpreted as a hallmark of hopping conductance since the contribution of extended carriers to  $\sigma_2$  is extremely small in the studied frequency domain.

An alternative scenario for low-temperature behavior of an interacting 2D system is formation of the Wigner crystal – periodic distribution of charge carriers.<sup>6</sup> In a pure electron system an interplay between the kinetic and interaction energy of electrons depends only on their density. At sufficiently low density, the typical interaction energy can exceed the Fermi energy of free electrons, and this is just the domain where the Wigner crystal can be formed.

Electron Wigner crystal was observed for the first on the surface of liquid He.<sup>7</sup> It was also identified in Si metal-oxide-semiconductor (MOS) structures with low electron concentration and high mobility, see Ref. 8 for a review.

External transverse magnetic field shrinks the electron wave functions and in this way facilitates formation of the Wigner crystal. As a result, in the presence of sufficiently strong magnetic field 2DEG can form the Wigner crystal even at relatively high electron concentration for which at  $B = 0$  the electron system is a liquid.<sup>9</sup> The Wigner crystallization in magnetic field was studied by many research groups, both experimentally and theoretically. Most of experiments were done using high-quality heterostructures such as  $n$ -GaAs/AlGaAs,<sup>10</sup> inversion high-mobility Si films,<sup>11</sup> InGaAs/InP heterostructures.<sup>12</sup> The most popular experimental method here is studies of DC  $I - V$  curves.<sup>8,11,12</sup>

The conventional point of view resulting from the above works is that in realistic 2D systems the Wigner crystal is strongly distorted by disorder and consists of correlated regions sometimes called ‘‘the domains’’. The whole structure is pinned by disorder forming a glass-like system see, e. g., Ref. 13. This *Wigner glass* should exhibit specific nonlinear and hysteretic response to the applied voltage, which is typical for pinned interacting random systems.<sup>14,15,16</sup> In the presence of AC excitation electrons vibrate around the pinning centers in a collective fashion forming the so-called *pinning collective mode* strongly influenced by the magnetic field. This mode was identified as a specific resonance in the AC conductance

observed in high-mobility  $n$  and  $p$ -GaAs/AlGaAs heterostructures at  $\nu < 0.2$ , i. e., in the EQL. The typical resonant frequencies were of few GHz.<sup>17,18,19,20</sup>

This work is aimed at studies of DC and AC magnetotransport in low-density heterostructures  $p$ -Si/SiGe ( $p = 8 \times 10^{10} \text{ cm}^{-2}$ ) both in the IQHE ( $\nu = 1$ ) and EQL regimes. In this material, the ratio between the typical hole-hole interaction energy and the Fermi energy is about 10; an additional advantage is that here formation of the Wigner crystal is not masked by the liquid phases corresponding to the fractional quantum Hall effect. In addition to conventional DC measurements, we measure velocity and attenuation of a surface acoustic wave (SAW) excited at the surface of a piezoelectric crystal located close to the 2D hole layer in the heterostructure. These measurements conducted at different temperatures and magnetic fields provide a probeless method for studying AC response. This method allows one determining the *complex* AC conductance, it has been previously successfully applied to  $n$ -GaAs/AlGaAs for identifying of Wigner crystal.<sup>21</sup> In this way we will demonstrate the evolution from metallic conductance at  $B = 0$  through hopping conductance in intermediate magnetic fields to formation of the Wigner glass in very high magnetic fields.

The paper is organized as follows. In Sec. II we report the procedures of measurement and data handling. The results are presented in Sec. III and discussed in Sec. IV.

## II. EXPERIMENT

### A. Procedure

We simultaneously measured attenuation and velocity of SAW in  $p$ -Si/SiGe heterostructures with hole density  $p = 8.2 \times 10^{10} \text{ cm}^{-2}$  and mobility  $\mu = 1 \times 10^4 \text{ cm}^2/\text{V}\cdot\text{s}$  in external magnetic field up to 18 T and temperature interval  $T = 0.3 - 4.2 \text{ K}$ . The measurements were performed in the frequency domain  $f = 18 - 255 \text{ MHz}$  using the so-called hybrid method, see, e. g., Ref. 5. According to this method, the SAW was excited by an inter-digital transducer at the surface of a piezoelectric crystal, LiNbO<sub>3</sub>, the heterostructure sample being pressed to the surface as illustrated on Fig. 1. The SAW generates a moving profile of electric field, which penetrates the 2D-interface, causing AC electric current. The current produces Joule heating, as well as feedback forces acting upon the elastic medium in the piezoelectric crystal. These processes result in an additional attenuation,  $\Delta\Gamma$ , of the SAW, as well as variation,  $\Delta v$ , of its velocity. Both effects depend on the conductance of the two-dimensional hole gas (2DHG) at the 2D interface. Consequently, by simultaneous measurement of  $\Delta\Gamma$  and  $\Delta v$  we extract *complex conductivity*,  $\sigma^{\text{AC}}(\omega) \equiv \sigma_1(\omega) - i\sigma_2(\omega)$ , of the 2D hole system versus magnetic field, temperature, and SAW amplitude. This ‘‘sandwich’’-like method allows to study non-piezoelectric systems by acoustic methods.

In addition to acoustic experiments, we measured components  $\rho_{xx}$  and  $\rho_{xy}$  of static electrical resistance, as well as the static current-voltage ( $I - V$ ) curves of a similar sample in magnetic field up to 18 T and temperatures  $T = 0.3 - 2.1$  K.

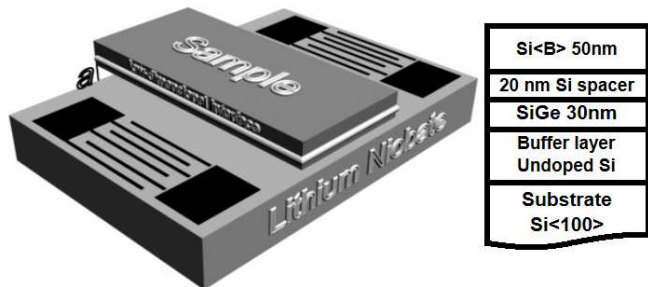


FIG. 1: Sketches of the acoustic experiment setup and sample.

The polymorphic fully strained heterostructure Si<B>/Si/SiGe/Si/(001)Si was grown using Solid Source MBE with e-beam on the substrate Si (100) (Fig. 1). It consisted of the 300 nm Si buffer layer followed by 30 nm Si<sub>0.92</sub>Ge<sub>0.08</sub> layer, 20 nm undoped spacer and 50 nm layer of B-doped Si with doping concentration  $2.5 \times 10^{18} \text{ cm}^{-3}$ . The 2D interface was located in the strained Si<sub>0.92</sub>Ge<sub>0.08</sub> layer, see Ref. 22 for detailed analysis of the sample.

The samples used for acoustic measurements were of the size  $0.3 \times 0.5 \text{ cm}^2$ . The DC measurements were performed using a satellite sample made from adjacent sector of the same heterostructure plate and shaped as a Hall bar. Sputtered Al strips annealed at  $500^\circ \text{ C}$  for 30 min served as Ohmic potential contacts, see Ref. 23.

### 1. Linear regime

*a. DC conductivity.* Shown in Fig. 2 is the temperature dependence of the static resistivity,  $\rho_{xx}$ , measured at  $B = 0$  and small measurement current (10 nA). This dependence corresponds to a metal-like behavior, the resistivity at the lowest temperature (0.3 K) being  $(7.5 \pm 0.1) \text{ k}\Omega/\square \approx 0.29 h/e^2$ . In this regime, the  $I - V$  curve remains Ohmic up the current of 300 nA. Thus, one concludes that at  $B = 0$  the hole system is in a metallic state even at the lowest studied temperature.

The components  $\rho_{xx}$  and  $\rho_{xy}$  were measured in the temperature domain 0.3 – 2 K and in magnetic fields up to 18 T ( $\rho_{xx}$ ) and 8 T ( $\rho_{xy}$ ). We were not able to measure  $\rho_{xy}$  in larger magnetic fields because there the  $\rho_{xx}$  turns out to be too large – 1.4 G $\Omega$  at  $T = 0.3$  K and measurement current  $I = 0.5$  nA. At such resistance the Hall voltage is masked by potential difference between the voltage probes along the  $\mathbf{x}$  axis.

The components of magnetoresistance versus magnetic field for  $B \leq 6$  T are shown in Fig. 3. One can notice a

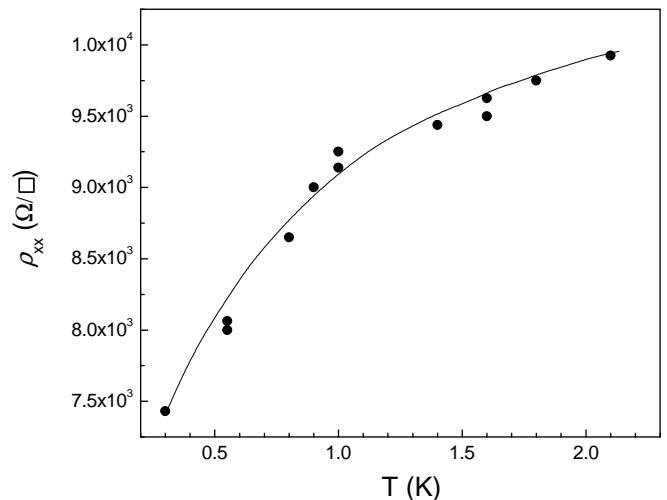


FIG. 2: Temperature dependence of static resistivity,  $\rho_{xx}$ ,  $B = 0$ ,  $I = 10$  nA. The line is a guide to eye.

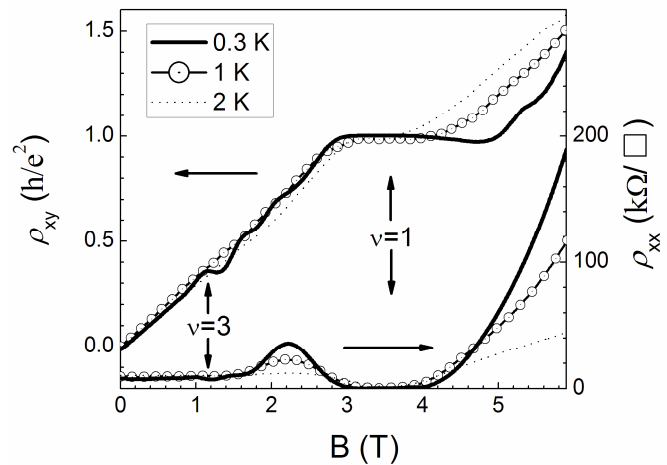


FIG. 3: Magnetic field dependences of  $\rho_{xx}$  and  $\rho_{xy}$  at different temperatures.

minimum in  $\rho_{xx}(B)$  due to the Shubnikov-de Haas (SdH) effect at the filling factor  $\nu = 1$ , as well as integer quantum Hall plateaus in  $\rho_{xy}$ . There is also a weak deep at  $\nu = 3$ , which is not clearly seen in Fig. 3 because of chosen scale. The absence of the minima for even values of the filling factor is usual for strained  $p$ -SiGe, see, e. g., Ref. 24 and references therein. The reason is the following. While the valence band in  $p$ -SiGe is 6-fold degenerate if both spin-orbit interaction and strain in the quantum-well structure are neglected the spin-orbit interaction plus strain partly lift the degeneracy leading to the energy separation of 23 meV between the heavy and light holes.<sup>24</sup> Therefore, the conductivity is maintained by the heavy holes. The spin splitting of the heavy holes in  $p$ -SiGe 2D-systems is significantly enhanced by exchange interaction. As a result, the spin splitting turns out to be close to the half of the cyclotron splitting,  $g^* \mu_B B \approx \hbar \omega_c / 2$ , where  $\omega_c = eB/m^*c$  is the cyclotron

frequency. This is why all even deeps are suppressed. This behavior strongly differs from that observed in the  $A^{III}B^V$  heterostructures.

At  $B \geq 4.5$  T and  $T \lesssim 10$  K the holes occupy the states only of lowest spin-split band of the 0-Landau level, so the condition of the quantum limit is fulfilled.

*b. Acoustic properties.* Shown in Fig. 4 are magnetic field dependences of the acoustic attenuation,  $\Delta\Gamma(B) \equiv \Gamma(B) - \Gamma(0)$ , and velocity,  $\Delta v(B)/v(0) \equiv [v(B) - v(0)]/v(0)$  at  $f = 87.7$  MHz. Here  $\Gamma(0)$  and  $v(0)$  are the SAW attenuation and velocity at  $B=0$ , respectively. One

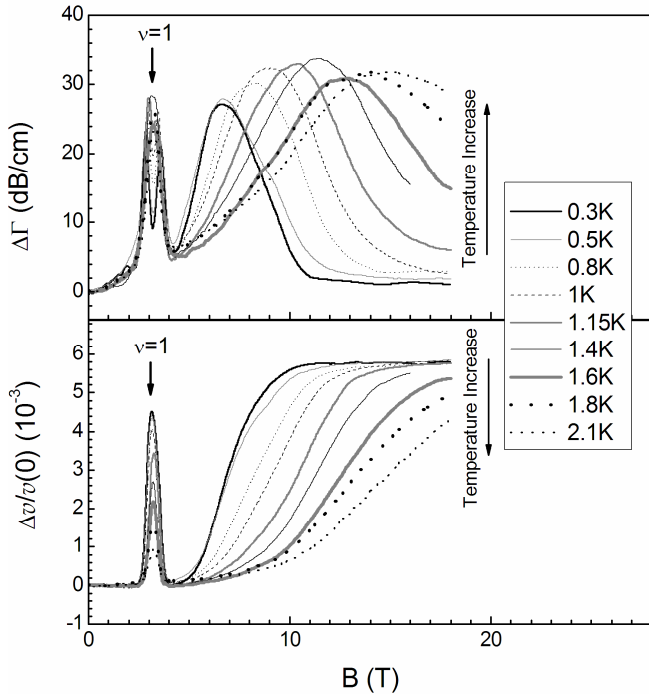


FIG. 4: Magnetic field dependences of  $\Delta\Gamma$  and  $\Delta v/v(0)$  for different temperatures.  $f = 87.7$  MHz,  $p = 8.2 \times 10^{10}$  cm $^{-2}$ .

can see pronounced extrema in both  $\Delta\Gamma$  and  $\Delta v/v(0)$  at the magnetic field corresponding to  $\nu = 1$ . These extrema coincide with the pronounced deep in static  $\rho_{xx}$ , Fig. 3. Above  $B \geq 4.5$  T the system is in the extreme quantum limit,  $\hbar\omega_c \gtrsim T$ . The curves measured at different frequencies (18, 30, 157, and 240 MHz) are similar.<sup>25</sup>

## 2. Nonlinear regime

*a. Voltage - current curves.* Shown in Fig. 5 are  $V - I$  curves for different temperatures and magnetic fields. One can see that the non-Ohmic behavior starts at very low current, the  $V - I$  curves being asymmetric with respect to the  $V$ -axis showing hysteresis at small currents, see Fig. 6. The sample resistance in the hysteretic region depends on the ramping rate. Note that the voltage-current curves show hysteretic behavior *only* in the domain of magnetic fields and temperatures where they are essentially *nonlinear*.

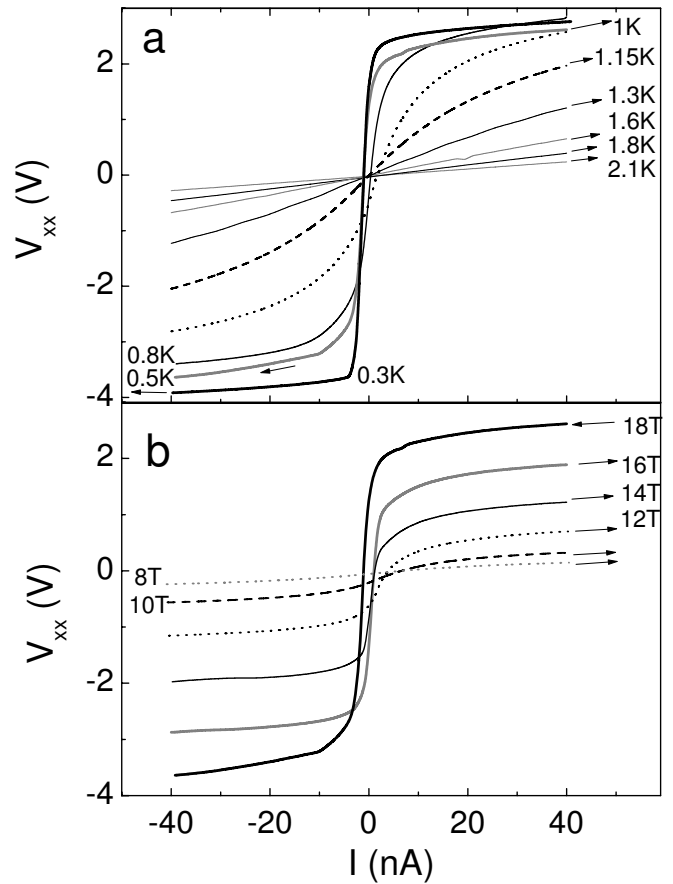


FIG. 5: (a) Voltage-current curves for  $B = 18$  T and different temperatures. (b) Voltage-current curves for  $T = 0.55$  K and different magnetic fields. The ramping speed is 5 nA/min. Arrows show the ramping direction.

*b. Acoustic properties.* The results of acoustic measurements for different SAW intensities are shown in Fig. 7. One can see that in the quantum-limit region,  $B \geq 4.5$  T, increase in the SAW intensity acts similarly to an increase in temperature. Namely, both the attenuation maximum and saturation of the SAW velocity shift towards large magnetic fields. Similar behaviors are observed at other SAW frequencies.

## B. Data handling

The components  $\sigma_{1,2}$  can be found from simultaneous measurement of  $\Delta\Gamma$  and  $\Delta v/v(0)$  by solving the set of

equations<sup>5</sup>

$$\frac{\Delta\Gamma \text{ (dB/cm)}}{8.68kA(k, a, d)} = \frac{\Sigma_1(B)}{[1 + \Sigma_2(B)]^2 + \Sigma_1^2(B)} - \frac{\Sigma_1(0)}{[1 + \Sigma_1(0)]^2 + \Sigma_1^2(0)}, \quad (1)$$

$$\frac{v(B) - v(0)}{v(0)A(k, a, d)} = \frac{1 + \Sigma_2(B)}{[1 + \Sigma_2(B)]^2 + \Sigma_1^2(B)} - \frac{1 + \Sigma_2(0)}{[1 + \Sigma_1(0)]^2 + \Sigma_1^2(0)} \quad (2)$$

where

$$\begin{aligned} A(k, a, d) &= 110.2b(k, a, d)e^{-2k(a+d)}, \\ \Sigma_i &= 4\pi t(a, k, d)\sigma_i/\varepsilon_s v(0); \\ b(k) &= (b_1(k)[b_2(k) - b_3(k)])^{-1}, \\ t(k, a, d) &= [b_2(k) - b_3(k)]/2b_1(k), \\ b_1(k, a) &= (\varepsilon_1 + \varepsilon_0)(\varepsilon_s + \varepsilon_0) \\ &\quad - (\varepsilon_1 - \varepsilon_0)(\varepsilon_s - \varepsilon_0)e^{-2ka}, \\ b_2(k, d) &= (\varepsilon_1 + \varepsilon_0)(\varepsilon_s + \varepsilon_0) \\ &\quad + (\varepsilon_1 + \varepsilon_0)(\varepsilon_s - \varepsilon_0)e^{-2kd}, \\ b_3(k, a, d) &= (\varepsilon_1 - \varepsilon_0)(\varepsilon_s - \varepsilon_0)e^{-2ka} \\ &\quad + (\varepsilon_1 - \varepsilon_0)(\varepsilon_s + \varepsilon_0)e^{-2k(a+d)}, \end{aligned} \quad (3)$$

$k$  is the SAW wave vector,  $d$  is the depth of the 2D-system layer in the sample,  $a$  is the clearance between the sample and the LiNbO<sub>3</sub> surface;  $\varepsilon_1=50$ ,  $\varepsilon_0=1$  and  $\varepsilon_s=11.7$  are the dielectric constants of LiNbO<sub>3</sub>, of vacuum, and of the semiconductor, respectively.

Utility of the above expressions is facilitated by the fact that at  $B = 0$  the conductance is metallic, and in the metallic state  $\sigma_1(\omega)$  is excellently approximated by the static conductance,  $\sigma^{\text{DC}}$ , for all relevant frequencies. Thus we can calibrate the AC response in the absence of magnetic field by the DC response. For example, for

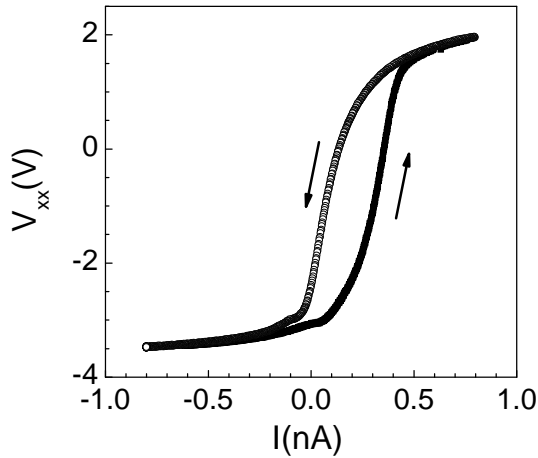


FIG. 6: Hysteretic  $V - I$  curves measured at  $T = 0.3$  K and  $B = 18$  T and ramping speed 0.1 nA/min. Arrows show the ramping direction.

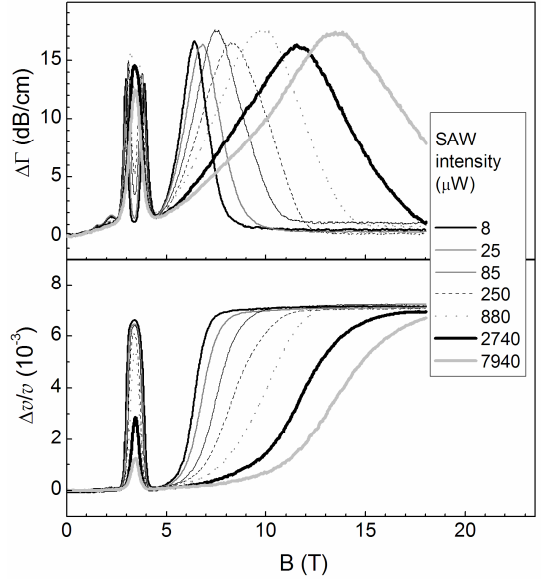


FIG. 7: Magnetic field dependence of  $\Delta\Gamma$  and  $\Delta v/v(0)$  at different RF-source powers.  $T = 0.3$  K;  $f = 30$  MHz.

$T = 0.3$  K we put  $\sigma_1|_{B=0} = \sigma^{\text{DC}}(0) = (1.33 \pm 0.02) \times 10^{-4} \text{ Ohm}^{-1}$ . The corresponding value of  $\Sigma_1$  for the relevant frequency range turns out to be much greater than 1. On the other hand, in the case of metallic conductance one can expect  $\Sigma_2 \ll 1$ .<sup>5</sup> Thus at  $B \rightarrow 0$

$$\frac{\Delta v(0)}{v(0)A(k, a, d)} \approx \frac{1}{1 + \Sigma_1^2} \rightarrow 0. \quad (4)$$

At  $B \rightarrow \infty$ , both  $\Sigma_1$  and  $\Sigma_2$  vanish and  $\Delta v/v(0)$  saturates at the value  $A(k, a)$ . That is exactly what we see in Fig. 4. Furthermore, we can find  $A(k, a)$  from the saturated value of  $[\Delta v/v(0)]_{B \rightarrow \infty}$ . Knowing  $k$ , we find from this quantity the thickness of the clearance,  $a$ . As an example, at  $T = 0.3$  K and  $f = 30$  MHz the saturated value of  $\Delta v/v(0)$  is  $7.16 \times 10^{-3}$  that corresponds to  $a = 4.3 \times 10^{-5}$  cm. We have checked that this value agrees with the results for different frequencies - 86, 144, 198, and 255 MHz - if the sample was not re-installed between the measurements. Figure 8 shows the saturation of the SAW velocity  $\Delta v/v(0)$  in high magnetic fields at different frequencies. Knowing  $a$ ,  $d$ , and  $\sigma^{\text{DC}}(0)$  we can calculate  $\Gamma(0)$ , and, respectively, find the absolute value of the SAW attenuation:  $\Gamma(B) = \Delta\Gamma(B) + \Gamma(0)$ . This is an important part of the procedure because in high magnetic fields we cannot find this quantity directly. Indeed, as one can see from Fig. 4, at large magnetic fields the quantity  $\Delta\Gamma$  is very small and the accuracy of its extraction from the raw AC data could be insufficient. Having determined the necessary parameters we then solve the set (1)-(2) for the quantities  $\sigma_1(\omega)$  and  $\sigma_2(\omega)$ .<sup>26</sup>

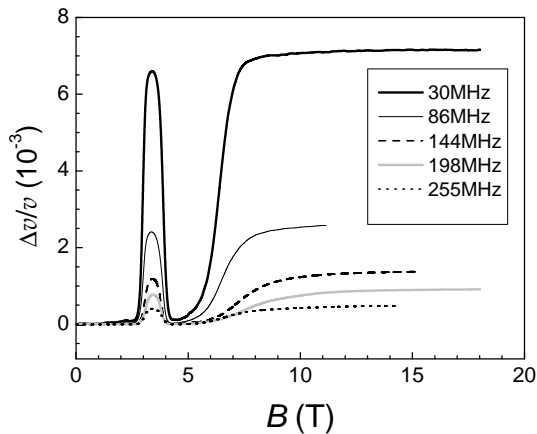


FIG. 8: The SAW velocity shift versus magnetic field at different frequencies at the same sample mounting,  $T=0.3$  K.

### III. RESULTS

#### A. QHE regime

Figure 9 illustrates experimental dependences of the real,  $\sigma_1$ , and imaginary,  $\sigma_2$ , components of the complex AC conductivity derived from the acoustical measurements using Eqs. (1) and (2), as well as of the DC-conductivity  $\sigma_{xx}^{\text{DC}} = \rho_{xx}/(\rho_{xx}^2 + \rho_{xy}^2)$ , on the reciprocal filling factor  $1/\nu \propto B$  at  $T=0.3$  K in the vicinity of the filling factor  $\nu = 1$ . As follows from this figure, outside

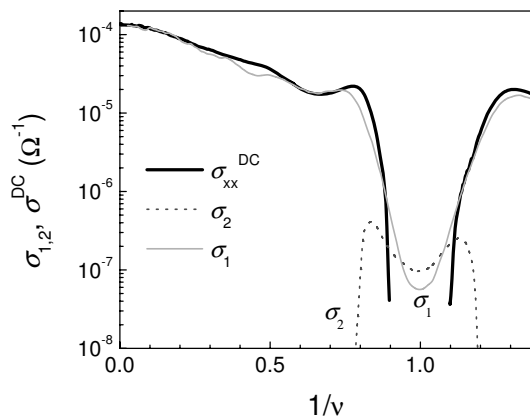


FIG. 9: DC conductivity and real & imaginary components of AC-conductivity at 30 MHz on the reversed filling factor in the vicinity of  $\nu = 1$ ;  $T = 0.3$  K.

the vicinity of  $\nu = 1$  the values of  $\sigma^{\text{DC}}$  and  $\sigma_1$  are close. This is exactly the region of metallic conductance where the hole states are extended. The situation dramatically changes close to  $\nu = 1$  where  $\sigma_1 \gg \sigma^{\text{DC}}$ . In addition, in this region the imaginary component,  $\sigma_2$ , of the AC conductivity becomes noticeable.

In Fig. 10, the components  $\sigma_1$  and  $\sigma_2$  are plotted as functions of temperature for  $B = 3.2$  T ( $\nu = 1$ ) and  $f =$

18 MHz. One can see that the ratio  $\sigma_1/\sigma_2$  increases with temperature. We believe that the low-temperature region where  $\sigma_2 > \sigma_1 > \sigma^{\text{DC}}$  corresponds to the hopping of the holes between localized states in the random potential produced by charged impurities.<sup>4</sup> We observe that the

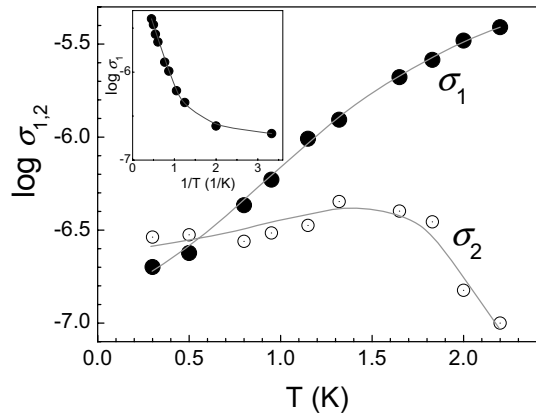


FIG. 10: Real and imaginary components of the AC-conductivity versus temperature for  $f = 18$  MHz and  $\nu=1$ . Inset: The Arrhenius plot ( $\log \sigma_1$  versus  $1/T$ ) for the same parameters.

AC hopping conductance is suppressed as temperature increases. At highest temperatures ( $T = 0.8 - 4.2$  K) the temperature dependence of  $\sigma_1$  is clearly governed by thermal activation,  $\sigma_1 \propto e^{-\Delta E/T}$ , with  $\Delta E \approx g^* \mu_B B$ , see inset in Fig. 10.

#### B. Extreme Quantum Limit

*c. Acoustic properties.* Shown in Fig. 11 is the dependence of  $\sigma_1$  at frequency  $f = 18$  MHz on inverse temperature,  $1/T$ , in different magnetic fields. We observe that at  $T = 0.8 - 2$  K and  $B = 8 - 18$  T the temperature dependence of  $\sigma_1$  is well described by the Arrhenius law,  $\sigma_1 \propto e^{-\Delta E/T}$ , with the activation energy,  $\Delta E$ , increasing with magnetic field, see inset. In this domain of temperatures and magnetic fields, for all the measured frequencies (18-87 MHz)  $\sigma_1 \approx \sigma^{\text{DC}}$  (measured for the current  $I = 0.5$  nA).

Both quantities depend on temperature according to the Arrhenius law, the activation energies being very close, see Fig. 11, inset. We believe that the observed activation dependences of  $\sigma_1$  and  $\sigma^{\text{DC}}$  are due to magnetic freeze-out of the holes from the extended states of the 0th Landau level to the states localized nearby the Fermi level. At low temperatures and large magnetic fields ( $T < 0.8$  K,  $B \geq 11$  T) the temperature dependence of  $\sigma_1$  becomes very weak.

Magnetic field dependences of  $\sigma_1$  at  $T = 0.3$  K and different frequencies as well as the DC conductivity measured with the current excitation of 0.5 nA are shown in Fig. 12.

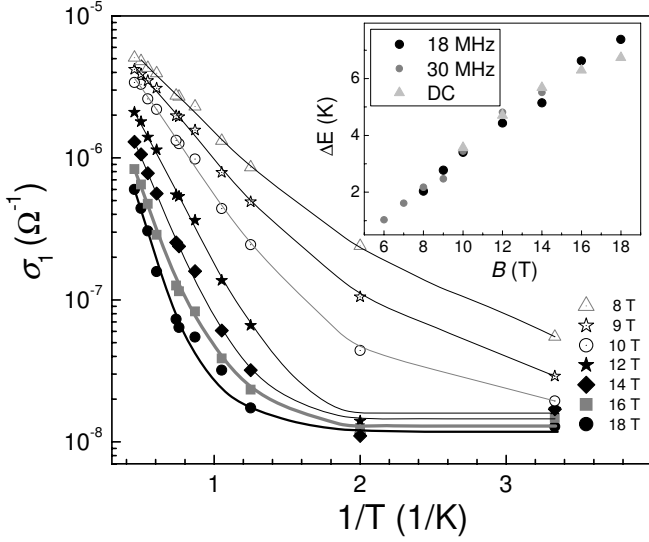


FIG. 11: Dissipative AC conductivity,  $\sigma_1$ , versus inverse temperature,  $1/T$ , for different magnetic fields.  $f = 18$  MHz, the lines are guides for eye. Inset: magnetic field dependence of the activation energy.

At  $B > 8$  T,  $\sigma^{\text{DC}}/\sigma_1 \ll 1$ ; this ratio can be less than 0.1. In addition, both the temperature and magnetic field dependences of  $\sigma^{\text{DC}}$  cannot be accounted for by conventional expressions for hopping conductance. The magnetic field dependence of  $\sigma_1$  weakens as magnetic field increases; at  $B \geq 12$  T the dependence is almost absent. Inset of Fig. 12 illustrates the frequency dependences of

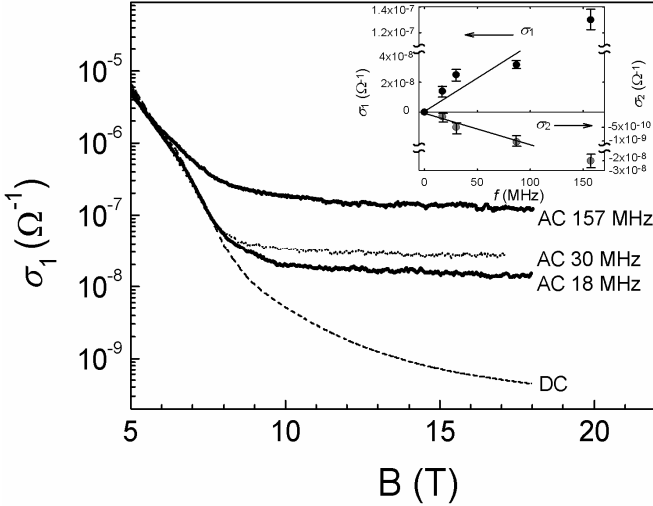


FIG. 12: Real part of the AC conductivity,  $\sigma_1$  at different frequencies and DC conductivity measured at 0.5 nA versus magnetic field;  $T = 0.3$  K. Inset: frequency dependences of  $\sigma_1$  and  $\sigma_2$  at  $B = 18$  T,  $T = 0.3$  K.

$\sigma_{1,2}$  at  $B = 18$  T and  $T = 0.3$  K. The low-frequency part of these dependences are *linear*:  $\sigma_{1,2}(\omega) \propto \omega$ . However, the slopes have different signs – the imaginary part of the conductivity,  $\sigma_2$ , is *negative*. The experimental points for

$f = 157$  MHz cannot be allowed for by the linear dependence, note that there is a break in the scale.

Shown in Fig. 13 are dependences of  $\sigma_1$  on the amplitude,  $E^{\text{AC}}$ , of the electric field produced by the SAW in the 2DHG. This amplitude is calculated from the expres-

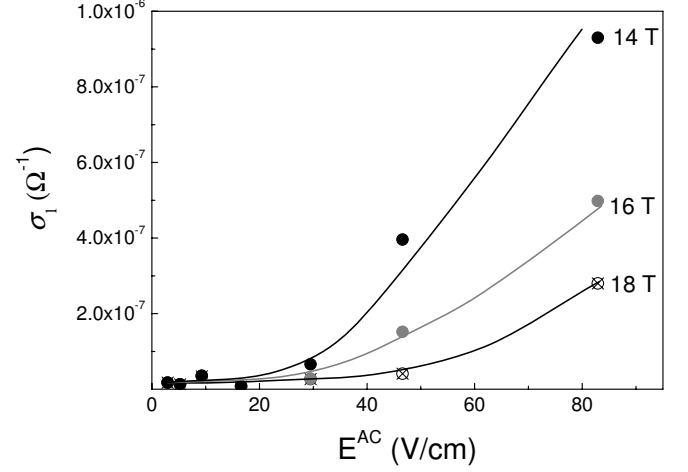


FIG. 13: Dependence of  $\sigma_1$  on the SAW amplitude,  $E^{\text{AC}}$ , at different magnetic fields.  $T = 0.5$  K,  $f = 30$  MHz. The lines are guides for eye.

sion<sup>27</sup>

$$(E^{\text{AC}})^2 = \frac{32\pi K^2}{v(0)} \frac{W}{l} e^{-2k(a+d)} \frac{kb(k, a, d)(\epsilon_1 + \epsilon_0)}{(1 + \Sigma_2)^2 + \Sigma_1^2}. \quad (5)$$

Here  $W$  is the acoustic power carried by the SAW,  $l$  is the SAW aperture. The rest of notations is the same as for Eqs. (1) and (2). Though the accuracy of this expression is not high one can still conclude that in strong magnetic field the nonlinear behavior starts at higher SAW intensities.

*d. DC measurements* Contrary to the case of AC conductance, the non-Ohmic behavior of the static  $V - I$  curves, Fig. 5, starts as a threshold. The threshold electric field,  $E_t$ , increases with the magnetic field. At  $B = 18$  T and  $T = 0.3$  K,  $E_t \approx 9$  V/cm. The threshold positions depend on the ramping speed of the current. However, even at the lowest ramping speed (0.02 nA/min) and smallest currents ( $I < 0.1$  nA) the  $V - I$  curves remain non-Ohmic. Thus one can conclude that the mechanisms of nonlinear behavior at zero and finite frequency are significantly different.

As we already mentioned, the  $V - I$  curves depend on the current ramping rate. To analyze the static nonlinear  $I - V$  curves it is convenient to plot them in the log-log scale. Shown in Fig. 14 is the log-log plot of  $V - I$  curves at  $B = 18$ ,  $T = 0.3$  K and different current sweep rate. The curve with the lowest ramping speed, 0.02 nA/min, can be fitted as

$$I \propto e^{-C/V^\alpha} \quad (6)$$

where  $C$  is a constant while  $\alpha = 0.3 - 0.4$ , see inset.

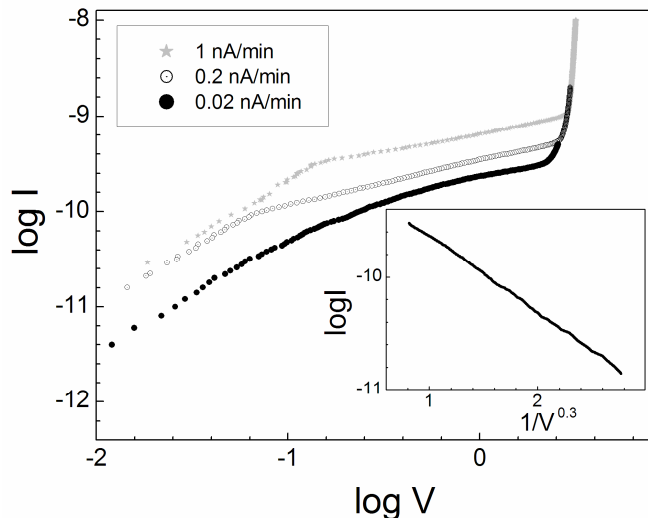


FIG. 14: log-log plot of the  $I$ - $V$ -curves with different current sweep rate at  $B = 18$ ,  $T = 0.3$  K. Inset: Logarithm of the current versus  $V^{-0.3}$  for the curve taken on the ramping speed 0.02 nA/min

#### IV. DISCUSSION AND CONCLUSION

From the experimental results and their analysis we conclude that the conduction mechanisms in  $p$ -SiGe heterostructures are different in different domains of temperature and magnetic field.

In the absence of magnetic field,  $B = 0$ , the conductance shows metallic behavior, see Fig. 4. In relatively weak magnetic fields, close to the filling factor  $\nu = 1$ , there is a temperature-driven crossover from the hopping conductance at low temperatures to the thermal activation at higher temperatures. Indeed, at low temperatures ( $T < 0.6$  K) both  $\sigma_1(\omega)$  and  $\sigma_2(\omega)$  relatively weakly depend on temperature, and the inequality  $\sigma_2 > \sigma_1 > \sigma^{DC}$  holds. This behavior is compatible with the predictions for hopping between the localized states created by the random impurity potential. The results in this domain of the magnetic field and temperature can be allowed for using conventional models for hopping conductance in 2D systems.<sup>4</sup> At  $T \gtrsim 1$  K,  $\sigma_2$  gets much less than  $\sigma_1$  and finally becomes not measurable, the temperature dependence of  $\sigma_1$  crosses over to the thermal activation (with magnetic field dependent activation energy). This behavior is typical for the conductance driven by extended states.

The extreme quantum limit occurs in very strong magnetic fields where  $\nu < 1$ . As follows from Fig. 3, the DC resistance at  $B \gtrsim 4.5$  T ( $\nu \lesssim 0.8$ ) becomes rapidly increasing with magnetic field. As the temperature increases, the temperature dependence of  $\sigma_1$  crosses over to thermal activation with magnetic field dependent activation energy, see Fig. 11. This behavior can be understood as a metal-to-insulator transition (MIT) driven by the magnetic field. A similar transition was observed

by many authors in  $p$ -Si/SiGe heterostructures, see, e. g., Ref. 24. A crossover from metallic to insulating behavior manifests itself also in the acoustic properties, as seen in Fig. 4 – at  $B \gtrsim 4.5$  T both  $\Gamma$  and  $\Delta v/v(0)$  cease to depend on temperature. With increase of temperature  $\sigma_1$  crosses over to the Arrhenius law, see Fig. 11. This law holds at  $T \gtrsim 1$  K for  $B = 18$  T and  $T \gtrsim 0.5$  K for  $B = 10$  T.

At the lowest temperature (0.3 K) and  $4.5 \text{ T} < B < 7 \text{ T}$ ,  $\sigma_1 > \sigma_2 > 0$ ,  $\sigma_1$  being almost independent of frequency, see Fig. 12. We believe that in this interval of magnetic fields the process of magnetic freeze-out takes place: occupation of extended states exponentially decreases with temperature, the activation energy increasing with magnetic field.

At very high magnetic field and low temperatures,  $B > 14$  T and  $T < 0.8$  K, we face rather unusual behavior. One could expect that at low temperatures and in very strong magnetic field the carriers are localized by a random potential, therefore both DC and AC conductance are due to single-particle hopping between the localized states. This would lead to an exponentially small Ohmic DC conductance,  $\sigma^{DC}$ , which should be much less than  $\sigma_1(\omega)$ . In addition, the predicted  $\sigma_2$  is positive, and it should significantly exceed  $\sigma_1$  in the whole studied frequency range.<sup>5</sup> Such a behavior was indeed observed in the vicinity of  $\nu = 1$ , i. e., in the integer quantum Hall effect regime. However, the experimental results for low temperatures and very high magnetic field strongly differ from these predictions. Indeed, the  $I$ - $V$  curves are nonlinear even for very small voltages. At larger voltages there is a pronounced increase in the current when the voltage exceeds some threshold value. The  $I$ - $V$  curves can be described by Eq. (6), which is typical for the creep motion of pinned charge density wave, or Wigner glass.<sup>14,15,16</sup> In the same region of temperatures and magnetic fields, the AC response is linear up to the electric field amplitudes,  $\sim 20$  V/cm;  $\sigma_1 \propto \omega$  is almost independent of temperature and magnetic field. The nonlinear effects are qualitatively similar to those caused by heating of carriers by the electric field created by the SAW. In addition, the imaginary part of the linear-response conductivity is *negative*, and  $|\sigma_2| \ll \sigma_1$  that contradicts to the predictions of the model allowing for the single-particle hopping.

We believe that the observed experimental results can be explained assuming that at low temperatures and in strong magnetic field the holes form a *Wigner glass*, i. e., a Wigner crystal distorted by disorder-induced pinning. Indeed, at small voltage and low temperature the pinned Wigner crystal should behave as an insulator. At finite temperature, parts of the Wigner glass experience correlated hops between different pinned states leading to the charge transfer. This process is similar to the *creep* of dislocations<sup>14</sup> or pinned vortices in type-II superconductors.<sup>15,16</sup> The law (6) and hysteretic  $I$ - $V$  curves are typical for the creep motion.

The dynamic response of weakly pinned Wigner crys-



tal at not too small frequencies is dominated by the collective excitations<sup>13,28</sup> where an inhomogeneously broadened absorption line (the so-called pinning mode) appears.<sup>29</sup> It corresponds to collective vibrations of correlated segments of the Wigner crystal around their equilibrium positions formed by the random pinning potential. The mode is centered at some disorder- and magnetic-field-dependent frequency,  $\omega_p$ ; its width being determined by a complicated interplay between different collective excitations in the Wigner crystal. There are modes of two types: transverse (magnetophonons) and longitudinal (magnetoplasmons). The latter include fluctuations in electron density. An important point is that pinning modifies both modes, and the final result depends on the strength and correlation length,  $\xi$ , of the random potential. Depending in the strength and correlation length of the random potential, the frequency,  $\omega_p$  may either increase, or decrease with magnetic field. As follows from experiments in GaAs,  $\omega_p \approx 10^{10} \text{ s}^{-1}$  ( $f \approx 1.5 \text{ GHz}$ ). Consequently, in our acoustic experiments  $\omega/\omega_p \ll 1$ . Hence, we were not able to observe the peak in the frequency dependence of the attenuation and can discuss only its low-frequency tail. The ratio  $\omega_p/\omega_c$  can be arbitrary. Depending on the interplay between the ratio  $\omega_p/\omega_c$  and the ratio  $\eta \equiv \sqrt{\lambda/\beta}$  between the shear ( $\beta$ ) and bulk ( $\lambda$ ) elastic moduli one can specify two regimes where the behaviors of  $\sigma^{\text{AC}}$  are different:

$$(a) 1 \ll \omega_c/\omega_{p0} \ll \eta, \quad (b) 1 \ll \eta \ll \omega_c/\omega_{p0}. \quad (7)$$

Here  $\omega_{p0}$  is the pinning frequency at  $B = 0$ . As a result, the variety of different behaviors is very rich. Assuming  $\xi \gg l_B = (\hbar c/eB)^{1/2}$  one can cast the expression for  $\sigma_{xx}(\omega)$  from Ref. 28 into the form

$$\sigma_{xx}(\omega) = i \frac{e^2 n \omega}{m^* \omega_{p0}^2} \frac{1 + iu(\omega)}{[1 + iu(\omega)]^2 - (\omega \omega_c / \omega_{p0}^2)^2}, \quad (8)$$

where the function  $u(\omega)$  is different for regimes (a) and (b). Note that the above equation differs from that of Ref. 28 by replacement  $\omega \rightarrow -\omega$ ,  $u \rightarrow -u$  since the sign of  $\omega$  used in the Fourier transform in Ref. 28 is opposite to that used in Eq. (2).

Below we will focus on the regime (b) since only this regime seems to be compatible with experimental results. Then

$$u(\omega) \sim \begin{cases} (\omega/\Omega)^{2s}, & \omega \ll \Omega, & (b1) \\ \text{const}, & \Omega \ll \omega \ll \omega_c. & (b2) \end{cases} \quad (9)$$

Here  $\Omega \sim \omega_{p0}^2 \eta / \omega_c$ , while  $s$  is some critical exponent. According to Ref. 28,  $s = 3/2$ . For the regime (b2) of Eq. (9) we have

$$\frac{\sigma_{xx}(\omega)}{\sigma_0} = \frac{\omega}{\omega_{p0}} \cdot \frac{i(1 + iu)}{(1 + iu)^2 - (\eta\omega/\Omega)^2} \quad (10)$$

where  $\sigma_0 \equiv e^2 p / m^* \omega_{p0}$ . The result can be cast in the

form

$$\sigma_1 = \sigma_0 u \frac{\omega}{\omega_{p0}} \frac{1 + u^2 + (\eta\omega/\Omega)^2}{[1 + u^2 + (\eta\omega/\Omega)^2]^2 - (2\eta\omega/\Omega)^2}, \quad (11)$$

$$\sigma_2 = -\sigma_0 \frac{\omega}{\omega_{p0}} \frac{1 + u^2 - (\eta\omega/\Omega)^2}{[1 + u^2 + (\eta\omega/\Omega)^2]^2 - (2\eta\omega/\Omega)^2}. \quad (12)$$

The above prediction is qualitatively compatible with the experimental results if one assumes

$$u \gg \omega \omega_c / \omega_{p0}^2 \gg 1. \quad (13)$$

Then

$$\sigma_1 \approx \sigma_0 \frac{\omega}{u}, \quad \sigma_2 = -\sigma_0 \frac{\omega}{u^2} \quad (14)$$

and  $\sigma_1/|\sigma_2| = u \gg 1$ . As follows from the experimental data (see inset of Fig. 12), the components  $\sigma_2 < 0$ , both  $\sigma_1$  and  $\sigma_2$  almost proportional to frequency, and their ratio is  $\sigma_1/|\sigma_2| \approx 40$ , i.e., greater than 1. In addition, the experimentally measured  $\sigma_1$  and  $\sigma_2$  are almost independent of magnetic field and temperature in the domain where we expect formation of the Wigner crystal.

The regime (14) requires the inequalities (13) and (9, b2) to be met simultaneously. These conditions impose restriction on the frequency  $\omega_{p0}$  of the collective mode. Indeed, they are both valid at the if  $\omega_{p0} \approx (1.2 - 1.5) \times 10^{10} \text{ s}^{-1}$ . In this way one can determine the pinning frequency in the absence of magnetic field. At  $\sigma_1/|\sigma_2| \approx 40$  and  $B > 14 \text{ T}$ , the inequality (13) is valid only for frequencies 18-90 MHz. At frequency  $f = 157 \text{ MHz}$ , the ratio  $\omega \omega_c / \omega_{p0}^2$  is much greater than 40. That can explain why the linear frequency dependence of  $\sigma_1$  and  $\sigma_2$  does not hold up to the highest experimental frequency. Taking into account low accuracy in determination of  $\sigma_2$ , the agreement between theory and experiment can be considered as satisfactory.

Assuming that  $\omega_{p0} = 1.5 \times 10^{10} \text{ s}^{-1}$ ,  $u = 40$  and using Eq. (8) one can estimate the concentration of the holes participating in formation of the Wigner crystal in the extreme quantum limit. The estimate yields a value, which is approximately by 2 orders of magnitude smaller, than the hole density in the absence of magnetic field ( $8.2 \times 10^{10} \text{ cm}^{-2}$ ). Apparently, in the very strong magnetic field most of carriers is captured by impurities and only small part is involved in formation of the Wigner glass. Unfortunately, we cannot compare this result with any data on Hall resistance,  $\rho_{xy}$ , since we were not able to measure this quantity in the extreme quantum limit.

Knowing the frequency  $\omega_{p0}$ , we can estimate the typical correlation length,  $L$ , of a pinned Wigner crystal. Following Ref. 30 we have

$$\omega_{p0} = c_t (2\pi/L), \quad (15)$$

where  $c_t = \sqrt{\beta/p m^*}$  is the velocity of transverse phonons in the Wigner crystal;  $m^*$  is the hole effective mass;  $\beta = 0.245 e^2 p^{3/2} / \varepsilon_s$  is the shear elastic modulus.

Assuming the effective hole density at  $T = 0.3 \text{ K}$  and  $B = 18 \text{ T}$  to be  $p \approx 10^9 \text{ cm}^{-2}$  (i. e., two orders lower

then 2DHG sheet density) one estimates the correlation length as  $L \approx 4 \times 10^{-4}$  cm. The lattice constant of the Wigner crystal  $a_W \equiv (\pi p)^{-1/2} \approx 4 \times 10^{-5}$  cm. Furthermore, with such  $p$  the ratio of the hole-hole interaction energy to the Fermi energy  $\kappa = E_{hh}/E_F \approx 70$ . Thus, the inequalities which are necessary conditions for the Wigner crystal formation –  $L \gg a_W$  and  $\kappa \gg 1$  – are met.

Though the above estimates produce reasonable numbers one should not overestimate their accuracy. The point is that, along with the “pinning” modes, there exist localized “soft” ones. They appear in the places where pinning is weak.<sup>13</sup> One can expect that these modes can also contribute to the AC conductance similarly as it happens in structural glasses.<sup>31</sup> Moreover, the frequency dependence of their contribution to  $\sigma_1(\omega)$  is close to linear, while the contribution to  $\sigma_2$  is small. Unfortunately, the density of these soft modes is unknown, therefore we are not able to estimate these contributions quantitatively.

To conclude the discussion, we believe that  $p$ -Si/SiGe heterostructures demonstrate crossover between different mechanisms of DC and AC conductance - from metallic conductance at  $B = 0$  through hopping in the integer quantum Hall effect regime to the pinned Wigner crystal (Wigner glass) in the extreme quantum limit (at  $B > 14$  T and  $T < 0.8$  K). The conclusion regarding formation of

the Wigner glass is supported by the behavior of complex AC conductance showing small negative imaginary part compatible with the predictions of Ref. 28 for the pinning mode of a Wigner crystal, as well as by a creep-like non-linear behavior and hysteresis of DC conductance. This conclusion agrees with that of Ref. 8 based on DC measurements.

### Acknowledgments

We are grateful to V.M. Pudalov and V. I. Kozub for useful discussions; to E. Palm and T. Murphy for their help with the experiments performed at the NHMFL.

The work is supported by grants of the Presidium of the Russian Academy of Science, the Program of Branch of Physical Sciences “Spintronika”, St. Petersburg Scientific Center of RAS 2007; NSF Cooperative Agreement No. DMR-0084173, State of Florida; NHMFL In-House Research Program. The work of YG, and VV was supported by the U. S. Department of Energy Office of Science through contract No. DE-AC02-06CH11357 and by Norwegian Research Council through USA-Norway bilateral agreement.

\* Electronic address: irina.l.drichko@mail.ioffe.ru

<sup>1</sup> “The Quantum Hall effect”, ed. by R. E. Prange and S. M. Girvin (Springer-Verlag, 1987).  
<sup>2</sup> L. D. Landau, E. M. Lifshits, *Kvantovaya Mehanika*, v.3, 1963, p.704, Moskva, Fizmatgiz.  
<sup>3</sup> O. Viehweger and K. B. Efetov, *J. Phys. Condens. Matter*, **2**, 7049 (1990); S. Kivelson, D.-H. Lee, and S.-C. Zhang, *Phys. Rev. B* **46**, 2223 (1992).  
<sup>4</sup> A. L. Efros, *Zh. Eksp. Teor. Fiz.* **89**, 1834 (1985) [*JETP* **89**, 1057 (1985)].  
<sup>5</sup> I. L. Drichko, A. M. Diakonov, I. Yu. Smirnov, Y. M. Galperin, and A. I. Toropov, *Phys. Rev. B* **62**, 7470 (2000).  
<sup>6</sup> E. Wigner, *Phys. Rev.* **46**, 1002 (1934).  
<sup>7</sup> C. C. Grimes and G. Adams, *Phys. Rev. Lett.* **42**, 795 (1979).  
<sup>8</sup> V. M. Pudalov, in: *Phys. of Quantum Sol. of Electrons*, 124 (1994), Int. Press.  
<sup>9</sup> Y. E. Lozovik and V. I. Yudson, *JETP Lett.* **22**, 11 (1975) [*Pis'ma Zh. Eksp. Teh. Fiz.* **22**, 26 (1975)].  
<sup>10</sup> H. W. Jiang, H. L. Stormer, D. C. Tsui, L. N. Pfeiffer, and K. W. West, *Phys. Rev. B* **44**, 8107 (1991).  
<sup>11</sup> V. T. Dolgoplov, G. V. Kravchenko, A. A. Shashkin, S. V. Kravchenko, *Phys. Phys. Rev. B* **46**, 13303 (1992).  
<sup>12</sup> B. Pödör, Gy. Kovács, G. Reményi, I. G. Savel'ev, and S. V. Novikov, *Inorg. Mat.* **37**, 439 (2001).  
<sup>13</sup> M. M. Fogler and D. A. Huse, *Phys. Rev. B* **59**, 2120 (1999).  
<sup>14</sup> L. B. Ioffe and V. M. Vinokur, *J. Phys. C* **20**, 6149 (1987).  
<sup>15</sup> M. V. Feigel'man, V. B. Geshkenbein, A. I. Larkin and V. M. Vinokur, *Phys. Rev. Lett.* **63**, 2303 (1989).  
<sup>16</sup> G. Blatter, M. V. Feigel'man, V. B. Geshkenbein, A. I.

Larkin, and V. M. Vinokur, *Rev. Mod. Phys.* **66**, 1125 (1994).  
<sup>17</sup> F. I. B. Williams, P. A. Wright, R. G. Clark, E. Y. Andrei, G. Deville, D. C. Glatli, O. Probst, B. Etienne, C. Dorin, C. T. Foxon, and J. J. Harris, *Phys. Rev. Lett.* **66**, 3285 (1991).  
<sup>18</sup> P. D. Ye, L. W. Engel, D. C. Tsui, R. M. Lewis, L. N. Pfeiffer, and K. West, *Phys. Rev. Lett.* **89**, 176802 (2002).  
<sup>19</sup> C. C. Li, J. Yoon, L. W. Engel, D. Shakhar, D. C. Tsui and M. Shayegan, *Phys. Rev. B* **61**, 10905 (2000). C. C. Li, L. W. Engel, D. Shakhar, D. C. Tsui and M. Shayegan, *Phys. Rev. Lett.* **79**, 1353 (1997).  
<sup>20</sup> P. Yong, G. Chen, G. Sambandamurthy, Z. H. Wang, R. M. Lewis, L. W. Engel, D. C. Tsui, P. D. Ye, L. N. Pfeiffer, and K. West, *Nature Physics* **2**, 452 (2006).  
<sup>21</sup> M. A. Paalanen, R. L. Willett, P. B. Littlewood, R. R. Ruel, K. West, L. N. Pfeiffer, and D. J. Bishop, *Phys. Rev. B* **45**, 11342 (1992).  
<sup>22</sup> L. Fedina, O. I. Lebedev, G. Van Tendeloo, J. Van Landuy, O. A. Mironov and E. H. C. Parker, *Phys. Rev. B* **61**, 10336 (1999).  
<sup>23</sup> S. Agan, O. A. Mironov, M. Tsaousidou, T. E. Whall, E. H. C. Parker, and P. N. Butcher, *Microelectronic Engineering* **51-52**, 527 (2000).  
<sup>24</sup> P. T. Coleridge, *Sol. St. Com.* **127**, 777 (2003).  
<sup>25</sup> Small ( $\leq 10\%$ ) difference in the peak positions can be attributed to the fact that the samples for DC and acoustic were cut from the neighbouring area of the heterostructure.  
<sup>26</sup> Note that the accuracy in determining of the clearance  $a$  strongly influences the obtained values of  $\sigma_2$  while  $\sigma_1$  is less sensitive to  $a$ .

- <sup>27</sup> I. L. Drichko, A. M. Diakonov, I. Yu. Smirnov, A. I. Toropov, *Semiconductors* **34**, 422 (2000) [*FTP* **34**, 436 (2000)].
- <sup>28</sup> M. M. Fogler and D. A. Huse, *Phys. Rev. B* **62**, 7553 (2000).
- <sup>29</sup> H. Fukuyama and P. A. Lee, *Phys. Rev. B* **17**, 535 (1977); *Phys. Rev. B* **18**, 6245 (1978).
- <sup>30</sup> B. G. A. Normand, P. B. Littlewood and A. J. Millis, *Phys. Rev. B* **46**, 3920 (1992).
- <sup>31</sup> S. Hunklinger and W. Arnold, in *Physical Acoustics*, edited by W. P. Mason and R. N. Thurston (Academic, New York, 1976), Vol. XII, p. 155; S. Hunklinger and A. K. Raychaudhuri, in *Progress in Low Temperature Physics*, edited by D.F. Brewer (Elsevier, Amsterdam, 1986), Vol. IX, p. 267.